Magnetic Resonance Imaging of Perfusion*

D. LE BIHAN

Diagnostic Radiology Department, The Warren Grant Magnuson Clinical Center, Building 10, Room 1C660, National Institutes of Health, Bethesda, Maryland 20892

Recent developments have shown that diffusion and blood microcirculation (perfusion) could be imaged and measured noninvasively by MRI. The purpose of this presentation is to overview the different approaches that use B_0 field gradients to monitor diffusion/perfusion. The principles of these different methods are discussed together with their limitations and their potential applications. © 1990 Academic Press, Inc.

INTRODUCTION

Considerable interest has recently emerged in the potential capability of magnetic resonance to image and measure blood flow at the capillary level—that is, tissue perfusion. Clinical interests have arisen in the characterization of pathological tissues by their capillary vasculature, follow-up of treatment by monitoring perfusion changes, and brain functional mapping associated with functional activity. Contrast-enhanced CT and angiography are currently used to evaluate tissue vasculature, while nuclear imaging methods such as positron emission tomography (PET) are fairly accurate for evaluating regional cerebral blood flow (rCBF) related to functional patterns. But the qualitative, invasive, and nonspecific nature of some of these methods or their cost makes alternative techniques desirable.

The sensitivity of MRI to spin motion has been well established and is frequently used for imaging blood flow in large vessels noninvasively. However, imaging and measuring blood flow at the capillary level is a considerably different challenge because the phenomena are much smaller. The capillary diameter is about 6 μm and the average velocity in the capillary network is in the range of 1 to 4 mm/s (*1*). For comparison, the diameter of the internal carotid artery is about 0.5 cm, and the average blood velocity within it is several tens of cm/s (*2*). However, it has been recently demonstrated that MRI can image perfusion (*3–7*). Except for techniques requiring tracers, which are described elsewhere, the different methods proposed to image perfusion are completely noninvasive and have in common the use of relatively strong magnetic field gradient pulses to encode slow flow. They give "perfusion" information somewhat different from that provided with the classical methods. Usually perfusion is quantified in terms of ml/min of blood per 100 g of tissue. Perfusion as seen by

---

* Presented at SMRM Workshop on MR Imaging of Blood Flow, Philadelphia, PA, March 13 and 14, 1989.

MRI, however, can be quantified in terms of active capillary density (ml of circulating blood/100 g of tissue) or average blood velocity (mm/s). Further assumptions about capillary bed structure are required in order to obtain results in ml/min/100 g. Another common problem is that microcirculation must be distinguished from other types of microscopic motion occurring in biological tissues, mainly molecular diffusion, and macroscopic motion, source of artifacts. Perfusion measurements could also be obtained using radiofrequency field (B_1) gradients (3) instead of magnetic field (B_0) gradients. However, since the equations of motion are nearly the same for B_1 and B_0 gradients, the approaches described in this paper may apply in both cases.

Microscopic imaging techniques may be capable of directly visualizing capillary microcirculation. With current medical imaging techniques, however, a typical voxel size is about 5 mm^3 (1 × 1 × 5 mm). It is obvious that such a voxel contains a large number of capillary segments, typically several thousand, so that microcirculation can be described as intravoxel motion. This occurs along with other types of microscopic motion, such as molecular diffusion (4). The topographic organization of the capillary network varies from species to species and between tissues. The brain capillary vasculature, for instance (1), may be described as a network of randomly oriented segments of about 60 μm radius of curvature. Direction of flow changes frequently (within seconds). A statistical description of both capillary geometry and capillary circulation is justified in most cases (muscle tissues where capillaries are typically roughly parallel may be an exception). Another important point is that only a fraction of the capillary volume may be functional at a given time. This fraction can dramatically increase when required by tissue metabolism (capillary recruitment), thus increasing the fractional volume occupied by flowing blood in voxels. Monitoring capillary volume evidently provides useful physiological information.

INTRAVOXEL MOTION AND MR IMAGING

If we consider the dephasing $\delta\Phi_j$ of the transverse magnetization of some population j of spins moving within the voxel during a time interval T, we obtain

$$\delta\Phi_j = \gamma \int_0^T v_j(t) \cdot G(t) t\, dt, \qquad [1]$$

where v_j and G are, respectively, instantaneous velocity and gradient vectors. The effect on overall flow-related dephasing Φ and amplitude F of transverse magnetization in a single voxel must take into account the distribution $p(\delta\Phi_j)$ of the dephasings in the voxel for the different populations:

$$F \cdot \exp(i\Phi) = \sum_j \exp(i\delta\Phi_j) \cdot p(\delta\Phi_j). \qquad [2]$$

Depending on capillary geometry and circulation conditions on the one hand and MRI acquisition parameters on the other, the effects on F and Φ may be very different. Perfusion can therefore be seen as an incoherent motion ($F < 1$, overall amplitude attenuation in the voxel) like molecular diffusion (5), as an incoherent motion that can be refocused in some circumstances ($F = 1$, $\Phi = 0$) (6), or as a coherent motion ($\Phi \neq 0$, overall dephasing in the voxel) (7).
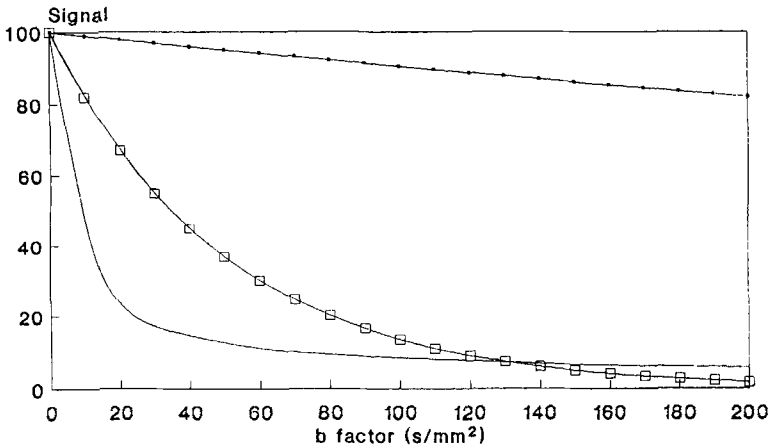
FIG. 1. Comparison of different microcirculation models. Signal attenuation due to microcirculation is reported as a function of the gradient factor b. Typical attenuation from diffusion, as expected in brain tissue ($D = 1 \times 10^{-3}$ mm^2/s), is indicated for comparison. According to data quoted in the text, the pseudo-diffusion coefficient associated with brain capillary perfusion in the case of the first model is about 20×10^{-3} mm^2/s. In the second perfusion model, the distribution of velocities is assumed to be Gaussian ($\langle v \rangle = 2.1$ mm/s, standard deviation $= 2$ mm/s), and the capillary segments are randomly oriented. It can be seen that in all cases, the attenuation caused by perfusion is larger than that caused by diffusion. Also, the two perfusion models have very similar effects, especially when $b > 100$ s/mm^2. (—●—) Diffusion; (□) pseudo-diffusion, first model; (—) pseudo-diffusion, second model.

A basic model of microcirculation would consider perfusion as microscopically incoherent. When the velocity v changes many times in direction during T, perfusion can be described as a random walk process, like molecular diffusion. In this case, it is easy to show that there is no overall dephasing ($\Phi = 0$) because motion is totally incoherent, but that the amplitude is attenuated by a factor F, where

$$F = \exp(-\langle \delta\Phi^2 \rangle) \qquad [3]$$

and $\langle \delta\Phi^2 \rangle$ is the variance of the dephasing distribution. According to this model, the effect of perfusion is a simple attenuation of the MR signal. This type of approach has been called intravoxel incoherent motion (IVIM) imaging (4, 5).

If one assumes that the distribution of the dephasings is Gaussian, one obtains

$$\langle \delta\Phi^2 \rangle = b \cdot (\langle l \rangle \cdot \langle v \rangle / 6), \qquad [4]$$

where b is a factor depending only on the gradient pulse sequence (cf. Appendix), $\langle l \rangle$ the average distance along which spins move with a constant velocity, and $\langle v \rangle$ that average velocity. The quantity ($\langle l \rangle \cdot \langle v \rangle / 6$) has the dimension of a diffusion coefficient and can be called a pseudo-diffusion coefficient D^*. Using the data quoted above for brain capillary circulation, one finds $D^* = 20 \times 10^{-3}$ mm^2/s, which is about 10 times larger than the true diffusion coefficient of water (Fig. 1). The similarity between diffusion and perfusion has allowed diffusion imaging to be successfully used for perfusion imaging (4, 5). Moreover, the difference in order of magnitude between D and D^* allows perfusion and diffusion to be separated on a quantitative

basis (5). Determination of D^* would give information on the capillary circulation type, combining geometry ($\langle l \rangle$) and dynamic ($\langle v \rangle$) properties.

Another model of incoherent microcirculation can be used when the velocity does not change direction or amplitude during the measurement time T, because spins stay in a straight capillary segment. In this case, relation [1] simplifies to

$$\delta\Phi_j = \mathbf{v}_j \cdot \left(\gamma \int_0^T \mathbf{G}(t)t\,dt \right) \equiv \mathbf{v}_j \cdot \mathbf{c}, \tag{5}$$

where

$$\mathbf{c} = \gamma \int_0^T \mathbf{G}(t)t\,dt. \tag{6}$$

Moreover, if we consider the angle Θ_j between the direction of the capillary segment and the gradient direction, then

$$\delta\Phi_j = c \cdot v_j \cdot \cos\Theta_j. \tag{7}$$

Again, the distribution of dephasings in the voxel must be taken into accoumt;

$$F \cdot \exp(i\Phi) = \int_0^\infty \int_0^\pi p(\Theta)p(v) \cdot \exp(ic \cdot v \cdot \cos\Theta) \sin\Theta\,d\Theta\,dv, \tag{8}$$

where Θ and v are considered independent variables, the distribution of which are $p(\Theta)$ and $p(v)$.

Assuming an isotropic orientation of the capillary segments, Eq. [8] becomes

$$F \cdot \exp(i\Phi) = \int_0^\infty p(v) \cdot \text{sinc}(cv/\pi)\,dv. \tag{9}$$

Here also, the result is a pure amplitude attenuation with no overall dephasing. Numerical calculation using the above data, and assuming $p(v)$ is Gaussian, shows that the order of magnitude of the signal attenuation is similar to that of the pseudo-diffusion model (Fig. 1), so that diffusion imaging techniques can again be used (5). In particular, using a Taylor expansion limited to the first orders of the sinc function, appropriate when cv is small, we obtain in the case of a plug flow velocity

$$F \approx 1 - (cv)^2/6 \tag{10}$$

while expansion to lowest order in the first pseudo-diffusion model leads to

$$F \approx 1 - b \cdot D^*. \tag{11}$$

The pseudo-diffusion coefficient D^* associated with the second model is thus

$$D^* \equiv v^2 \cdot [c^2/(6b)]. \tag{12}$$

It is worth noting that the pseudo-diffusion coefficient now depends only on the dynamic property of the capillary network ($\langle v \rangle$) and no longer on its geometry (assuming isotropic capillary orientation). D^* depends now also on the acquisition sequence parameters and more particularly on the measurement time (cf.

Appendix), whereas the pseudo-diffusion coefficient of the first model is constant, as a true diffusion coefficient.

A final point concerning intravoxel motion is that the flowing component constitutes only a limited, usually small, fraction of the voxel volume. If f is this fractional volume, in other words, the active capillary density in ml/mg of tissue, the voxel transverse magnetization is

$$M_{xy\,\text{voxel}} = [(1 - f) \cdot M(T1_s, T2_s, D_s)] + [f \cdot F \cdot \exp(i\Phi) \cdot M(T1_c, T2_c, D_c)], \quad [13]$$

where subscripts s and c, respectively, refer to the "static" and the circulating components. This expression assumes there are no other effects than relaxation, diffusion, and perfusion. In particular, effects of exchanges between capillaries and tissues are neglected, as are the effects of blood flow in greater vessels in the voxel. Also, T1 and T2 in the static and the flowing component are often supposed to be similar to a first approximation (5, 6), which may be disputable. Differences in T2 may also be used to distinguish the flowing from the static component (7).

Let us now consider three different approaches which have been proposed for perfusion imaging, according to expected values for F and Φ.

PERFUSION IMAGING

Intravoxel Incoherent Motion Imaging

IVIM imaging is based on diffusion imaging techniques. The effect of molecular diffusion in the presence of magnetic field gradients is a pure amplitude attenuation B, such that

$$B = \exp(-b \cdot D), \quad [14]$$

where b is the gradient factor mentioned above (cf. Appendix) and D the diffusion coefficient. Diffusion images are thus generally calculated from at least two spin-echo sequences, (S_1) and (S_2), which are differently sensitized to diffusion by additional gradient pulses (4, 8, 9),

$$D(x, y, z) = \log[M_1(x, y, z)/M_2(x, y, z)]/(b_2 - b_1), \quad [15]$$

where b_2 and b_1 are the gradient factors and M_2 and M_1 the transverse magnetizations associated with sequences S_2 and S_1, respectively. T1 and T2 effects are eliminated by using in (S_1) and (S_2) the same acquisition parameters (TR, TE). Other sequence schemes have also been proposed, such as sequences involving stimulated echoes (10), steady-state free precession (10, 11), or echo-planar imaging EPI (13–15), but the basic principles are the same.

When microcirculation effects are present, however, the image calculated using [15] is no longer a simple diffusion image, but depends also on perfusion. That is why the term apparent diffusion coefficient (ADC) has been suggested to characterize such images (4, 5). IVIM images can thus be used to give information on both diffusion and perfusion. Obviously, the ADC is an artificial parameter and has no intrinsic physical significance; characterization of the attenuation decay as a function of the gradient factor b would give more useful information. In particular, three fundamental parameters, i.e., diffusion coefficient D, perfusion attenuation F, and capillary
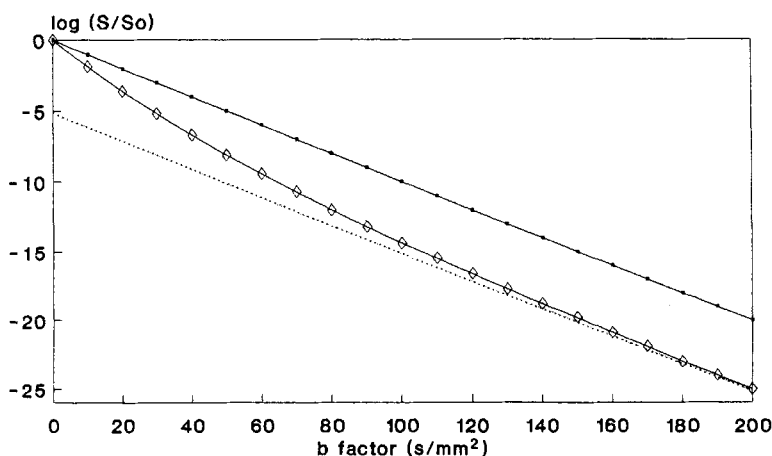
FIG. 2. Model of voxel. In a voxel, effects of both the flowing component and the static component must be taken into account. The first perfusion model was used (D^* = 20 $\times$ 10^{-3} mm^2/s) in this simulation. The capillary volume is typically 5 ml/100 mg of tissue. The logarithm of the signal attenuation is plotted against the b factor. The overall effect of perfusion is to shift the attenuation curve by a quantity log(1 $-f$), so that the intercept gives the perfusion factor f. The slope of the attenuation curve, as measured with large b values ($b >$ 100 s/mm^2) gives the diffusion coefficient D. Perfusion and diffusion effects may be integrated in the "apparent diffusion coefficient," which is the slope of the attenuation curve obtained for smaller b values (typically between 0 and 100 s/mm^2). (■) Diffusion only; (◇) diffusion + perfusion; ($\cdots$) asymptote to diffusion.

density f, would be separately determined. Unfortunately, the precise determination of three unknown variables requires many acquisitions with different b values, incompatible with clinical requirements due to lengthy acquisition times. Single-shot imaging techniques (13–15) may change this situation. Nevertheless the ADC concept has proved to be handy when perfusion is evaluated from IVIM images calculated from only two acquisitions. If certain hypotheses are made regarding tissue parameters and appropriate acquisition parameters are used, it can be shown from [13] and [15] that the contribution of perfusion to the ADC does not depend on the capillary network geometry and blood velocity, but only on the capillary density f (4):

$$\text{ADC} \approx D + f/b_2. \tag{16}$$

This relation mainly depends upon the order of magnitude difference expected between diffusion and perfusion effects as mentioned above. Using typical values for D, f, and b_2 (1 $\times$ 10^{-3} mm^2/s, 5%, and 100 s/mm^2, respectively), it appears that the perfusion term is about 30% of the ADC and thus a significant part of it, although the fraction of flowing spins is very small (Fig. 2). Moreover, separate images of diffusion (D) and perfusion (f) can be obtained using two IVIM images acquired with different values for b_2 (5), but an accurate determination of these variables would require much more points in order to establish the full attenuation curve.

Refocusing Imaging Techniques

In the case of the second model of incoherent flow described above, the term incoherence refers to the whole voxel because of the random orientation of the capillary

segments (macroscopic incoherence). It is obvious, however, that flow may be considered coherent for spins moving and staying inside a given capillary segment during T (microscopic coherence). If their velocity is constant during T, the even-echo rephasing phenomenon occurs, so that each $\delta\Phi_j$ is zero on even echoes. It results that the overall dephasing in the voxel is canceled out and that there is no attenuation from flow on such echoes. Ahn *et al.* proposed to use this feature to map capillary perfusion (6). In this technique, two spin-echo sequences sensitized to slow flow are compared as for IVIM imaging, but one of them is a double echo sequence. These two sequences are designed in such a way that effects of diffusion, T1, and T2 are identical for corresponding signals. The perfusion map is calculated by subtracting the image of the single echo sequence from the image of the second echo of the double echo sequence, so that static spins are eliminated. This perfusion map depends on both capillary density and velocity distribution, but because it derives from subtraction and not the ratio of the acquired images, there is also some dependence in T1, T2, and diffusion. Therefore, quantification of perfusion cannot be done easily, although this method may provide useful qualitative images of capillary microcirculation. Improvements on this method, however, may enable one to obtain a pure capillary density map.

A potentially useful alternative to this method, valid also in the case of the second type of incoherent motion, is to compare two sequences sensitized to slow microscopic motion, one of which has been compensated for constant flow by an appropriate design of its gradient pulses (16, 17). Diffusion effects are eliminated if the noncompensated sequence and the compensated sequence have exactly the same diffusion weighting. Unfortunately, the succession of positive and negative gradient pulses required for flow-compensation purposes considerably reduces the value of the gradient factor b, so that very large gradient pulses are needed to keep the same diffusion effects. This kind of approach has the potential to distinguish between the two types of microcirculation (microscopically coherent or incoherent) because no refocusing can be obtained for completely incoherent motion.

Intravoxel Coherent Motion (IVCM) Imaging

A third approach, proposed by Young *et al.* (7), is to allow for some macroscopic coherence in perfusion flow, so that a net flow can be detected in the voxel. The average flow-related dephasing in the voxel therefore differs from zero. In this case, phase-sensitive reconstruction processes may allow access to perfusion. In practice, the same method designed for IVIM imaging is used, except that the phases rather than the amplitudes of the two sequences differently sensitized to perfusion are taken into account (7). Quantification of flow is, however, difficult to obtain because calculation of the average dephasing in a given voxel depends not only on the dephasing produced by the fraction of coherently moving spins but also on the fraction of incoherently moving spins and the fraction of static spins, for both of which dephasing is null. The last component is also largely predominant, so that the overall voxel dephasing does not reflect accurately the dephasing produced by the flowing component. Contribution of the static component may be reduced by using long echo times. Perhaps more interesting is that, depending on the direction of the gradient pulses used, the direction of the average flow in a voxel can in principle be determined.

Comparison of the Three Approaches—Clinical Applications

The successful use of the three types of methods described above demonstrates that coherent and incoherent effects can both be found in microcirculation. Indeed, the method to be used should be chosen according to the tissue in which perfusion measurements are carried out. For instance, in muscles or in kidney cortex where capillaries are mainly parallel, coherent flow is likely to predominate. Refocusing and IVCM imaging techniques may thus be more appropriate. In other tissues, such as brain, where the capillary network is essentially randomly organized, flow is mainly incoherent, at least at the macroscopic level, so that IVIM imaging may be more efficient. The presence of coherent components seen with IVCM imaging might be related to the presence of flow in other, larger vessels than capillaries. Refocusing techniques can still be used if microcirculation is coherent at the microscopic level. The velocity must therefore be constant in direction and amplitude during the measurement time T (typically echo time TE). According to data quoted earlier for brain tissue, this condition should occur when T does not exceed 30 ms at best (i.e., when there is no acceleration), which is quite short and difficult to achieve because of time needed to insert motion-probing gradient pulses in the sequence. Moreover, simulation shows that the pseudo-diffusion model applies as soon as four or more changes in velocity direction occur, so that the IVIM technique works for any types of capillary geometry.

The common drawback of these three approaches is the frequent occurrence of artifacts related to eddy currents, gradient instabilities, and object motion. Additional fluctuation dephasings generated by object motion or gradient instabilities may severely impair perfusion images. In the case of motion artifacts, if motion is spatially coherent, the effect is a pure overall dephasing in all voxels. The dephasing is constant if motion is also temporally coherent (gating techniques may be required). (This does not affect techniques based on amplitude measurements such as IVIM imaging.) On the other hand, techniques that generate perfusion images from phase measurements should correct for this additional source of dephasing. In all cases, use of single-shot imaging techniques, such as EPI, when configured for diffusion/perfusion imaging purposes (*14, 15*), should solve this problem.

Despite the above limitations, perfusion/diffusion images have already been obtained in clinical practice, mainly using the IVIM concept in brain (*4, 5*). A distinction can easily be observed between diffusion measurements in liquid structures such as cysts, and to some extent in extracellular edema, where diffusion is free and comparable to that in pure water, and measurements in solid tissues, where diffusion is usually restricted by the presence of microscopic barriers and measured diffusion coefficients are found to be reduced by about a factor two. This restricted diffusion effect may also be anisotropic, such as in brain myelin fibers (*18*). Large differences have also been found in ADC measurements that have been proven to be related to perfusion, allowing highly perfused tumors to be identified by patterns different from those of poorly perfused tumors. Abnormalities in diffusion/perfusion images have also been detected when regular T1- and T2-weighted images failed (*5*). Furthermore, as the capillary bed is directly involved in IVIM images, discrepancies may be observed when compared to constrast-enhanced MRI, such as in images enhanced by gadolinium, where perfusion is indirectly visualized, depending on the integrity of the blood–brain barrier. Perhaps the most exciting area is imaging of brain activity

as it varies according to physiological or pathological conditions. Despite low spatial resolution, variations in cerebral blood flow with external stimulations have been shown using PET. It would be interesting to get such results using the high spatial resolution of perfusion MRI without tracer. However, improvements in signal-to-noise ratios and temporal resolution are a necessary first step before such goals can be accomplished.

APPENDIX: CALCULATION OF THE GRADIENT FACTOR b

The value of the gradient factor b involved in diffusion and perfusion effects is defined by

$$b(T) = \int_0^T k^2(t)dt, \qquad \mathbf{k} = \gamma \int_0^t \mathbf{G}(t')dt'. \qquad [A1]$$

In the case of a spin-echo sequence, this relation must be slightly modified to take into account the 180° dephasing imposed by the 180° pulse at $t = \text{TE}/2$ (G must be transformed in $-G$ for $t > \text{TE}/2$).

A first consequence of Eq. [A1] is that the gradient axes used for imaging can be considered independently because they are perpendicular, so that their contribution to the b factor is purely additive, i.e., $b = b_x + b_y + b_z$, when diffusion is isotropic. For anisotropic diffusion, one must rewrite Eq. [14]:

$$B = \exp[-(b_x D_x + b_y D_y + b_z D_z)]. \qquad [A2]$$

A second result is that the contribution of the different gradient pulses which are on the same axis cannot be considered independently in all cases. In particular, if the diffusion-probe gradients are on the readout gradient between the predephasing and the readout gradient pulses, the effects of these last pulses cannot be neglected in the b calculation even if their amplitude is very small as compared to the diffusion gradient pulses, because of the presence of cross terms.

In the case where only two identical diffusion gradient pulses (amplitude G, duration d) separated by a time interval I are present, Eq. [A1] leads to

$$b = \gamma^2 \cdot G^2 \cdot d^2 \cdot [I + 2d/3] \qquad [A3]$$

which is the well-known relation established by Stejskal and Tanner (*19*). With the same pulse scheme, the c factor defined in the text is

$$c = \gamma \cdot G \cdot d(I + d). \qquad [A4]$$

The quantity $[c^2/(6b)]$ involved in the pseudo-diffusion coefficient of the second microcirculation model is thus

$$(I + d)^2/[6(I + 2d/3)] \qquad [A5]$$

and is a pure temporal parameter, independent of G.

REFERENCES

1. G. PAWLIK, A. RACKL, AND R. J. BING, *Brain Res.* **208**, 35 (1981).
2. D. J. BRYANT, J. A. PAYNE, D. N. FIRMIN, AND D. B. LONGMORE, *J. Comput. Assist. Tomogr.* **8**, 588 (1984).
3. G. S. KARCZMAR AND M. E. MOSELEY, *in* "Proceedings, Seventh SMRM," p. 727, August 1988.
4. D. LE BIHAN, E. BRETON, D. LALLEMAND, P. GRENIER, E. CABANIS, AND M. LAVAL-JEANTET, *Radiology* **161**, 401 (1986).
5. D. LE BIHAN, E. BRETON, D. LALLEMAND, M. L. AUBIN, J. VIGNAUD, AND M. LAVAL-JEANTET, *Radiology* **168**, 497 (1988).
6. C. B. AHN, S. Y. LEE, O. NALCIOGLU, AND Z. H. CHO, *Med. Phys.* **14**, 43 (1987).
7. I. R. YOUNG, A. S. HALL, D. J. BRYANT, *et al., J. Comput. Assist. Tomogr.* **12**(5), 721 (1988).
8. D. LE BIHAN AND E. BRETON, *C. R. Adad. Sci.* [*II*] *(Paris)* **301**, 1109 (1985).
9. D. G. TAYLOR AND M. C. BUSHELL, *Phys. Med. Biol.* **30**, 345 (1985).
10. K. D. MERBOLDT, W. HANICKE, AND J. FRAHM, *J. Magn. Reson.* **64**, 479 (1985).
11. D. LE BIHAN, *Magn. Reson. Med.* **7**, 346 (1988).
12. D. LE BIHAN, R. TURNER, AND J. MACFALL, *Magn. Reson. Med.* **10**, 324 (1989).
13. H. E. AVRAM AND L. E. CROOKS, *in* "Proceedings, Seventh SMRM," p. 980, August 1988.
14. R. TURNER AND D. LE BIHAN, *J. Magn. Reson.*, in press.
15. R. TURNER, R. VAVREK, J. MAIER, AND D. LE BIHAN, *in* "Proceedings, Eigth SMRM," p. 1123, August 1989.
16. J. F. MAKI, G. P. COFER, AND G. A. JOHNSON, *Radiology* **16**(P), 155 (1988).
17. C. THOMSEN, P. RING, AND O. HENRIKSEN, *in* "Proceedings, Seventh SMRM," p. 890, August 1988.
18. M. E. MOSELEY, Y. COHEN, J. MINTOROVITCH, L. CHILEVITT, H. SHIMIZU, J. TSURVDA, et al., in "Proceedings, Eight SMRM," p. 136, August 1989.
19. E. O. STEJSKAL AND J. E. TANNER, *J. Chem. Phys.* **42**, 288 (1965).